White Rose Research Online

eprints@whiterose.ac.uk
https://eprints.whiterose.ac.uk
Universities of Leeds, Sheffield and York

Deposited via The University of Sheffield.

White Rose Research Online URL for this paper:
https://eprints.whiterose.ac.uk/id/eprint/238339/

Version: Published Version

Article:
Hallett, D., Wiercinski, J., Hallacy, L. et al. (2026) Controlling coherence between waveguide-coupled quantum dots. Physical Review Applied, 25 (2). L021003. ISSN: 2331-7019

https://doi.org/10.1103/1xsb-bf5r

Reuse
This article is distributed under the terms of the Creative Commons Attribution (CC BY) licence. This licence allows you to distribute, remix, tweak, and build upon the work, even commercially, as long as you credit the authors for the original work. More information and the full terms of the licence here: https://creativecommons.org/licenses/

Takedown
If you consider content in White Rose Research Online to be in breach of UK law, please notify us by emailing eprints@whiterose.ac.uk including the URL of the record and the reason for the withdrawal request.

UNIVERSITY OF LEEDS
University of Sheffield
UNIVERSITY of York

Letter

Controlling coherence between waveguide-coupled quantum dots

D. Hallett,[1,*] J. Wiercinski,[2,†] L. Hallacy,[1] S. Sheldon,[1] R. Dost,[1] N. Martin,[1] A. Fenzl,[1] I. Farrer,[3] A.K. Verma,[3] M. Cygorek,[4] E.M. Gauger,[2] M.S. Skolnick,[1] and L.R. Wilson[1]

[1] *School of Mathematical and Physical Sciences, University of Sheffield, Sheffield S3 7RH, United Kingdom*
[2] *SUPA, Institute of Photonics and Quantum Sciences, Heriot-Watt University, Edinburgh EH14 4AS, United Kingdom*
[3] *School of Electrical and Electronic Engineering, University of Sheffield, Sheffield S1 3JD, United Kingdom*
[4] *Condensed Matter Theory, Department of Physics, TU Dortmund, 44227 Dortmund, Germany*

(Received 11 April 2025; revised 18 September 2025; accepted 14 January 2026; published 17 February 2026)

We present a waveguide design incorporating a split-diode structure, allowing independent electrical control of transition energies of multiple emitters over a wide range with minimal loss in waveguide coupling efficiency. We use this design to systematically map out the transition from superradiant to independent emission from two quantum dots through control of the emitter detuning. We perform both lifetime and Hanbury Brown-Twiss measurements on the device, observing antidips in the photon coincidences—indicating collective emission, while at the same time observing a drop in lifetime around zero detuning—indicating superradiant behavior. Performing both measurements allows us to investigate detuning regions, which show both superradiant rate enhancement and interemitter coherence, as well as regions in which correlations persist in the absence of rate enhancement.

DOI: 10.1103/1xsb-bf5r

Introduction. Multiple indistinguishable quantum emitters can couple to an optical mode as a single entity [1], experiencing enhanced light-matter coupling [2] and creating strongly correlated emission [3]. Such coherent interactions between quantum emitters are vital for the scaling up of many quantum information schemes [4,5]. Optical coupling between multiple quantum emitters enables the generation of light with nonclassical photon statistics [6–8] entanglement between qubits [9–12], and advanced quantum photonic circuits [13,14]. Moreover, quantum enhancement of the light-matter interaction is the basis for superabsorbers for light harvesting and quantum batteries [15], while the concomitant effect of subradiance can protect quantum memories against losses [16,17], and enable long-range exciton transfer [18,19].

The most prominent effect of collective light-matter coupling is superradiance, which emerges if an ensemble of identical emitters couples to the electromagnetic field. Superradiance manifests in a scaling of the emitted light intensity, $\langle I(t)\rangle \propto N^2$ [1,20]. For two emitters [cf. Fig. 1(a)], superradiance leads to enhanced transitions via a collective superposition state, the bright state $|B\rangle$, with rate Γ_B, while a dark state, $|D\rangle$, decouples from the electromagnetic field and decays with reduced rate Γ_D [21,22]. Taking into account only the decay of the single-excitation manifold, a linear increase in the emission rate is observed [cf. Fig. 1(c)] [23]. Introducing a detuning between the emitters leads to coherent oscillations between the dark and the bright states, until the detuning is significantly larger than the light-matter coupling, in which case the system behaves as two individual emitters decaying with individual rates γ_1 and γ_2 [cf. Fig. 1(b)].

Additionally, interemitter coherences are created by the transitions between delocalized states [24,25]. These can be measured using Hanbury Brown-Twiss (HBT) experiments, and result in a characteristic antidip observed in the two-photon correlations at zero delay time [cf. Fig. 1(d)]. Of note, the antidip in the HBT signal results from relating the emission of a detected photon to a transition via a correlated emitter state (the bright state). Such a transition can also be engineered for spatially separated, nonsuperradiant emitters via erasure of which-path information in the measurement process [25–29].

Self-assembled quantum dots (QDs) have emerged as a leading platform for demonstrating and controlling quantum photonic effects such as superradiance—combining the practicality of realizing solid-state emitters at fixed

*Contact author: d.hallett@sheffield.ac.uk
†Contact author: J.Wiercinski@hw.ac.uk

Published by the American Physical Society under the terms of the Creative Commons Attribution 4.0 International license. Further distribution of this work must maintain attribution to the author(s) and the published article's title, journal citation, and DOI.

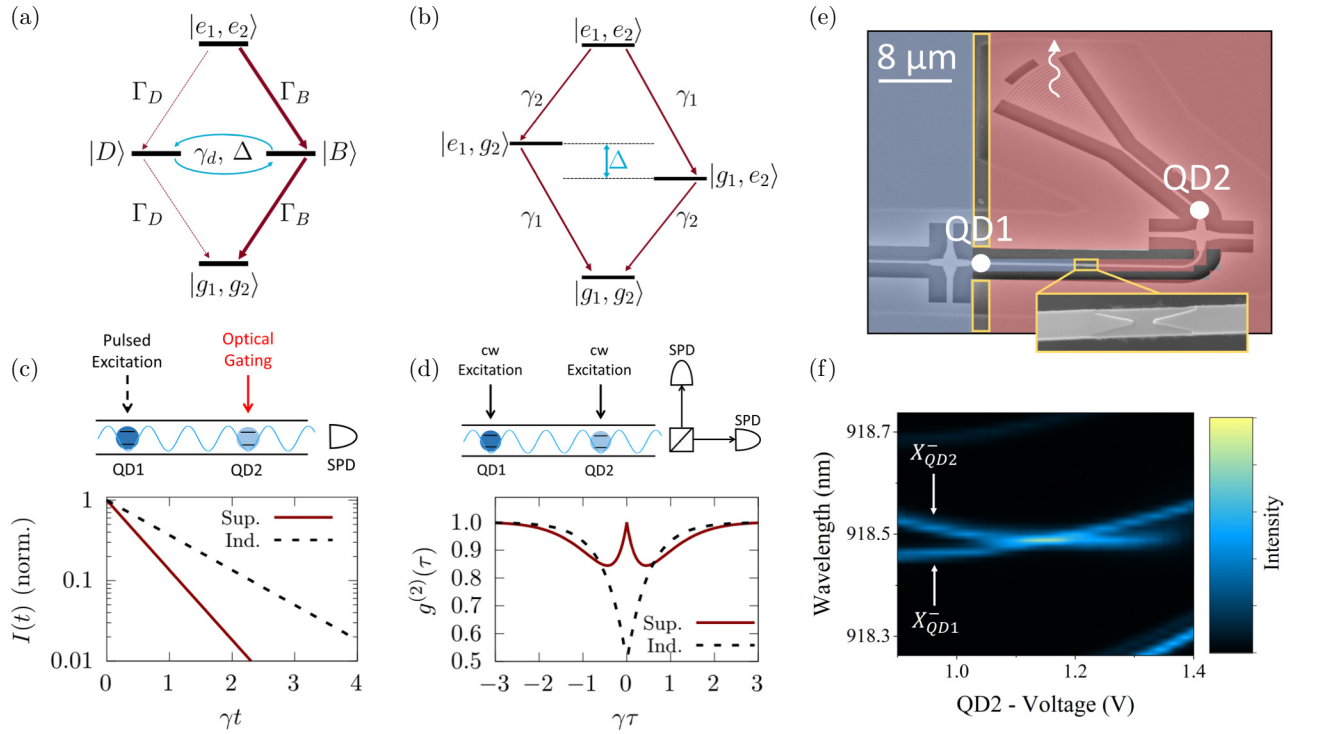

FIG. 1. Independent tuning of QDs and properties of superradiant emission. (a) Energy-level diagram of two resonant waveguide-coupled QDs. The states $|e_1, e_2\rangle$ and $|g_1, g_2\rangle$ describe both QDs in their excited and ground states, respectively. The spectral detuning and dephasing rate are labeled Δ and γ_d. (b) Energy-level diagram of two independent quantum emitters. The state $|e_1, g_2\rangle$ ($|g_1, e_2\rangle$) signifies that X^-_{QD1} (X^-_{QD2}) is excited, while the other QD is in the ground state. (c) Expected intensity decay for an ideal system of two superradiant (solid red line) or two independent (dashed black line) emitters given the depicted excitation scheme. (d) Expected autocorrelation function $g^{(2)}(\tau)$ for a pair of superradiant (solid red line) or independent (dashed black line) emitters given the depicted excitation scheme. (e) SEM image of the waveguide device. The positions of the two QDs are marked by white spots. The red and blue coloring marks the area of the two diodes that control the two QDs. Yellow indicates the areas that are etched for electrical isolation. Inset: SEM of the isolation etch in the waveguide. (f) Emission spectrum of the X^- transitions of the two QDs, measured from the outcoupler of the device, as a function of the voltage applied to QD2 [red area in (e)].

positions with excellent optical properties [30,31] and integrability into nanophotonic devices [32,33]. Nevertheless, there are several challenges to overcome in order to scale up superradiant solid-state quantum devices. First, QDs typically grow with random sizes and geometries, which makes it necessary to tune different QDs into resonance, for example, through control of temperature [26, 34], strain [35], magnetic field [21], or electric field [28]. However, these tuning methods can be slow, irreversible, or nonscalable. Second, superradiance requires spatial indistinguishability of the quantum emitters, while quantum dots occupy separate positions within a solid-state structure. An attractive solution to achieve superradiance between spatially separate solid-state emitters is therefore to coherently couple them to a photonic structure such as a waveguide [34,35]. This facilitates an effective coupling to a set of confined one-dimensional optical modes, leading to the emergence of coherent QD-QD superposition states. Depending on the distance between the QDs, this waveguide-mediated coupling leads to an energy splitting between those coherent states (dispersive regime), or to enhanced radiative–superradiant–decay along one of the coherent superposition states (dissipative regime) [21,36–39].

Existing experimental work on superradiance in solid-state emitters has used either the change in decay rate and the presence of a dark state [21], or photon coincidence measurements [34,35,40] to demonstrate the presence of superradiance. For this, mostly the case of zero detuning has been compared to a far-detuned case, in which the emitters are assumed to behave independently. However, quantitative changes in the photon emission rate may have origins different from superradiance, e.g., variations of the dipole of a single emitter resulting from changes of the wave function upon tuning, or contributions from dark exciton states [32]. An antidip observed in HBT experiments could, in principle, be used to indicate the presence of coherence between the QDs at resonance but not necessarily superradiance [28]. Therefore, it is desirable to measure both photon coincidences as well as changes in the

lifetime, while continuously varying the detuning between the QDs to demonstrate the presence of superradiance.

Here, we demonstrate measurements of both lifetimes and photon coincidences on two independently tuneable QDs coupled to a nanobeam waveguide across a wide range of spectral detunings. Independent tuning of the QDs is achieved by separate electrical gating [41]. This gating method allows fast, repeatable tuning of individual emitters, without compromising transmission through the photonic device, while at the same time being scalable to larger QD numbers. Optical gating of one QD [42,43] is used to switch between—and therefore directly compare—superradiant and nonsuperradiant regimes, by effectively adding and removing one emitter. Measurements of the decay rate of the system indicate a clear enhancement of the decay rate when the emitters are resonant. Additionally, we confirm the presence of strong QD-QD correlations by performing HBT experiments, even at detunings much larger than multiple single-emitter linewidths.

Device design. The device studied in this work is pictured in Fig. 1(e). Two InAs QDs are coupled to a nanobeam waveguide that supports a single guided TE mode. The waveguide is a suspended beam 280 nm wide and 170 nm thick, and is terminated at both ends by shallow-etch grating couplers. The positions of the two QDs are marked by white circles. The distance between the QDs is approximately 20 μm—roughly 70× the wavelength of light in the waveguide. The two QDs can be separately addressed using two driving lasers, and emission is collected from the grating outcoupler at the end of the waveguide.

In this work, we use separate Stark tuning of the two sections to control the detuning between the transitions of the QDs. To achieve this, the QDs are located in a split diode structure, allowing different voltages to be applied to different sections of the device. The membrane consists of a *p*-*i*-*n* diode with AlGaAs tunneling barriers to increase the QD tuning range (see the Supplemental Material [44]). A shallow etch is used to break electrical conductivity through the top *p*-doped layer of the diode, allowing different voltages to be applied to the separate regions. The positions of this etch are marked in yellow in Fig. 1(e), and the red and blue coloring indicates the two electrically isolated regions. The geometry of the shallow etch through the waveguide is optimized using finite-difference time-domain simulations and adjoint-based [45,46] inverse design to minimize loss; an SEM image of the shallow waveguide etch is inset in Fig. 1(e). The outcome of this optimization is presented in the Supplemental Material, where we estimate that the electrical isolation etch results in a $<1\%$ transmission loss across a broad bandwidth [44]. At the same time, from numerical simulations we expect this waveguide design to achieve a coupling efficiency (β factor) of around 0.8. This beta factor could allow for state-of-the-art quantum dots [47] to achieve a lifetime reduction of about 42%, close to the maximum of 50% [44].

Relative tuning of the negatively charged trions of the two QDs ($X^-_{\mathrm{QD1,QD2}}$) is shown in Fig. 1(f). The trion states are identified by the lack of fine-structure splitting, and high turn-on voltage. For this measurement, both QDs are excited using above-band lasers and emission is collected from the outcoupler. The voltage applied to QD1 is held constant at 1.17 V. The voltage applied to QD2 [the red section in Fig. 1(e)] is tuned, blueshifting the emission from X^-_{QD2} as the voltage is increased. It can be seen that X^-_{QD1} is also tuned, due to crosstalk between the two diodes, with X^-_{QD1} redshifting with increasing voltage. At approximately 1.15 V the two transitions are near degenerate.

Lifetime measurements. First, we explore the radiative decay dynamics of the system using the excitation scheme shown in Fig. 1(c). The X^-_{QD1} state is excited with an above-band femtosecond pulse, emission is collected from the outcoupler and correlated with the time of the laser pulses to generate the emission decay curve. The effect of the second QD is controlled by optically gating the X^-_{QD1} transition using a weak (100 nW) continuous-wave above-band laser. This optical gating effect has been demonstrated in several studies on resonant excitation [42,43,48]. This gating laser prepares QD2 in the ground state of the X^-_{QD2} transition, without significantly exciting the X^-_{QD2} state. The detuning between the states is controlled by tuning the voltage applied to QD1. Each measurement is taken with and without the optical gating laser, allowing us to directly compare the voltage-dependent decay dynamics of QD1 with the coupled two QD system.

The resulting decay curves are presented in Fig. 2(a). From panel (i), it is apparent that the decay is faster with X^-_{QD2} active and degenerate with X^-_{QD1}. This enhanced decay is very sensitive to detuning, and reduces continuously (ii)–(iii) until at detunings beyond just 0.5 GHz (iv) the presence of QD2 no longer affects the decay rate.

The decay of superradiant emitters is not expected to follow a simple exponential decay [21]. Therefore, we use thresholds to assess the change in decay time. In particular, we consider the time $\tau(\epsilon)$ it takes for the intensity to decay from its maximum value I_0 to a threshold of ϵI_0, where $\epsilon = 1/2, 1/e, 1/10$.

The detuning dependence of the decay times to these three thresholds is shown in Fig. 2(b). Considering first only the results for X^-_{QD1} (darker colored lines), the decay gradually gets quicker as the QD is tuned to positive detunings. This is most clear in the 1/10 (red) threshold. We attribute this to a change in the QD dipole as it is tuned. There is also a slight rise of between 5% and 10% in the decay times for some thresholds around $\Delta = 0$. A mono-exponential fit to the data (see Supplemental Material [44])

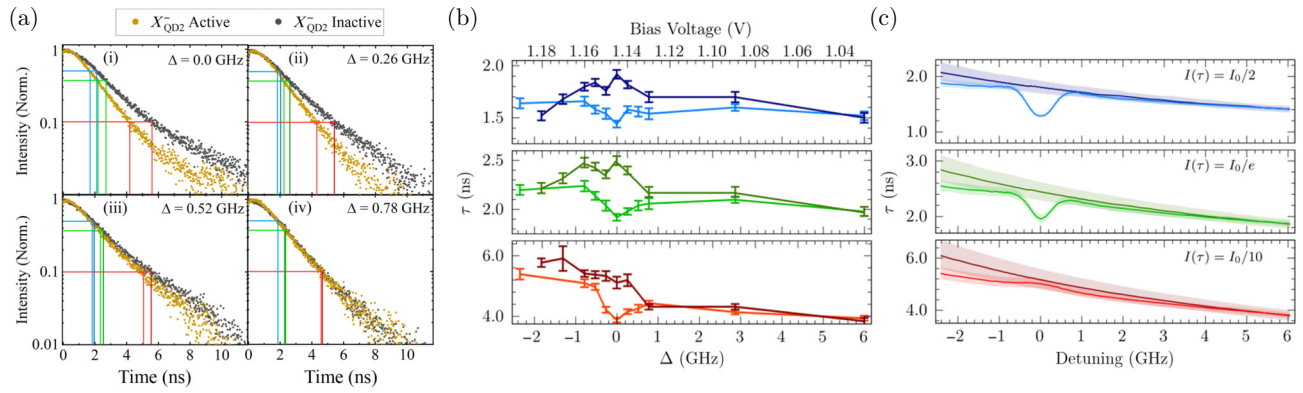

FIG. 2. Enhancement of emitter decay rate. (a) Comparison of the decay curves of the system with the QDs detuned by (i) $\Delta = 0$, (ii) $\Delta = 0.26$ GHz, (iii) $\Delta = 0.52$ GHz, and (iv) $\Delta = 0.78$ GHz. Measurements are performed with (yellow) and without (black) optical gating of QD2. Colored lines indicate where the intensity drops below the thresholds used in (b),(c). (b) Detuning dependence of the decay rate with (lighter lines) and without (darker lines) gating of QD2. The results are plotted as the time taken for the emission intensity to drop below three threshold values: $I_0/2$ (blue), I_0/e (green), and $I_0/10$ (red). (c) Theoretical prediction of the results in (b). The shaded regions signify uncertainties in the model due to errors in the X^-_{QD1} lifetime estimation.

indicates a monotonic tuning response. We therefore attribute the nonmonotonic behavior of the decay times to the timing jitter introduced by the nonresonant excitation.

Comparing this to the case where X^-_{QD2} is active [lighter lines in Fig. 2(b)], we see that X^-_{QD2} has little effect on the decay dynamics when the states are detuned. At resonance however, we see a significant reduction of about 20% in decay time. We attribute this to a superradiant enhancement of the bright state decay rate Γ_B with respect to the single QD decay rate γ_1. Ideal superradiance would lead to a reduction of the decay time by 50%. This is not observed in this sample due to a combination of nonunity beta factor, and line-broadening effects, like spectral wandering and other dephasing sources, e.g., phonons [22,44]. We have developed a theoretical model that provides quantitative insights into the impact of these detrimental effects. The experimental data is consistent with a dissipative coupling to the waveguide modes. However, the phase delay cannot be estimated precisely because its impact is masked by the line broadening. We obtain good qualitative agreement between theory and experiment with a beta factor of $\beta = 0.8$ and spectral line broadening due to slow energy fluctuations with a standard deviation of $\sigma = 0.3$ GHz [see Fig. 2(c)]. A quantitative analysis of these various influences is provided in the Supplemental Material [44]. While we obtain good agreement between theory and experiment for short and medium times, we observe differences at long times [see lower panels in Figs. 2(b) and 2(c)]. At long times, the intensity is predicted to be dominated by the presence of the dark state, leading to an increase in decay time [see Fig. 2(c), lower panel]. Note that this biexponential behavior of the intensity has been seen in previous experiments [21] but is not visible in our experimental data. We attribute this discrepancy to nonradiative decay processes, which dominate over the small dark-state decay rate and provide a more detailed theoretical analysis in the Supplemental Material [44]. Overall, the lifetime measurements reveal that the emission behavior of the sample is altered by optically activating X^-_{QD2}. These alterations are significant in the region around zero detuning and lead to a consistent reduction of the observed decay times, indicating a superradiant enhancement.

Photon coincidence measurements. In addition to the measurements of decay times presented in the previous section, HBT experiments are performed on the same pair of QDs. Signals from N distinguishable single-photon sources exhibit a dip to $g^2_{\text{ind.}}(0) = 1 - N^{-1}$, with a width that is determined by the radiative lifetime of both QDs [49]. Interemitter coherence, on the other hand, produces an antidip with a width determined by the coherence time of the emitter. These measurements allow a direct observation of interemitter coherence during the emission process [25,29]. In this way, the presence of interemitter coherences can be validated as the cause of the radiative lifetime results in the previous section. For this, both QDs are excited continuously with above-band cw lasers leading to incoherent population of the two negatively charged trions (X^-_{QD1},X^-_{QD2}). Emission is collected from the out coupler, spectrally filtered to isolate emission from the two QDs, split using a beam splitter, and sent to two single-photon detectors (SPDs). The detuning of the emitters is controlled by tuning the voltage across QD1.

The results of the HBT experiments for different detunings can be seen in Fig. 3. For large spectral detunings (top panel) the QDs show uncorrelated emission signified by a drop of the second-order autocorrelation function to 0.5 at zero time delay. By contrast, when both QDs are tuned into resonance (bottom panel), an antidip approaching unity

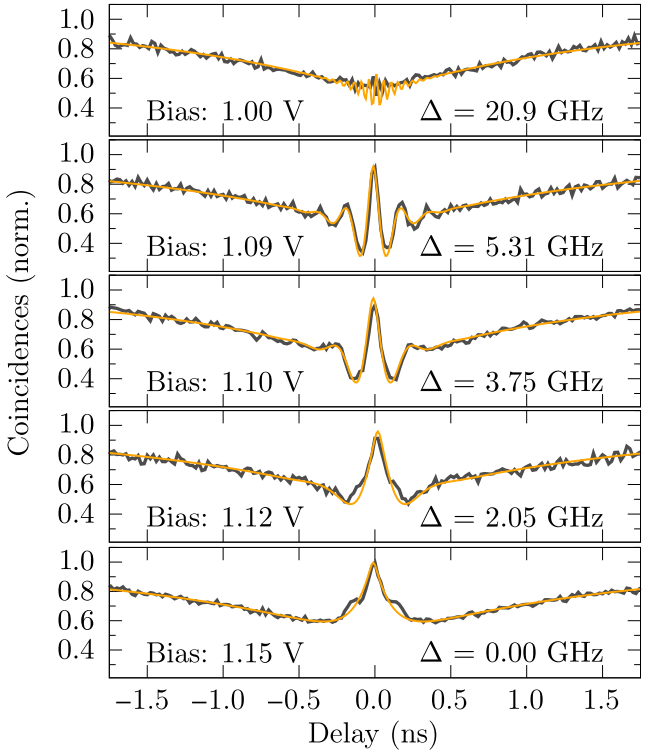

FIG. 3. Photon correlations. Autocorrelation function of emission collected from the end of the waveguide as a function of emitter-emitter detuning. The yellow lines are theoretical predictions of the measurements.

at zero delay time can be observed, which indicates the presence of interemitter coherence after the first photon emission, i.e., the preparation of the bright state by the emission process. At intermediate detunings, a beating behavior is observed with a beating frequency $f = \Delta/h$ given by the detuning between the QDs. This is caused by an oscillation of the relative phase of the QDs, which leads to the collective bright state evolving into the dark state and back [44]. Interestingly, coherence in the emission process can still be observed at detunings far larger than the single-emitter linewidth, and exceeding the region of rate enhancement that has been observed in lifetime measurements [see Fig. 2(a)]. The transition between the correlated emission at zero detuning and uncorrelated emission can be explained by the beating frequency increasing, until it can no longer be resolved by the measurement. Using the measured spectral detuning as a parameter without fitting, our theoretical model captures the transition between correlated and independent emission and reproduces the height and frequency of the beating with an estimate of spectral wandering of $\sigma = 0.3$ GHz and a pure dephasing rate of $\gamma_d = (8.0 \pm 1.6)$ ns^{-1}, which are identical across all HBT experiments [44]. The pure dephasing and spectral wandering would likely be improved by using resonant excitation, but that was not possible in this sample.

Discussion. In this work we have presented a gated architecture combined with an optimized waveguide design that enables precise, independent control of emitter wavelengths while maintaining high coupling efficiencies to the waveguide optical modes. This control is fast, reversible, and easily scalable. This design was used to create and control coherence between two QDs at a distance 70 times larger than the emission wavelength. This work utilizes randomly positioned QDs with a density of 10 QDs/μm^2. From this density we estimate a device yield of 0.9 QD pairs per device, although this yield drops quickly when attempting to make devices with more than two QDs [44]. Combining the split-contact technique with a deterministic method for positioning emitters within photonic structures [50–53], would allow a truly scalable quantum dot platform to be realized.

We have performed combined HBT and lifetime measurements on two QDs embedded in a waveguide device. Systematically tuning the QDs in and out of resonance, we demonstrated the transition from a superradiant system to fully independent emitters. At low to zero detuning we demonstrate a decrease in lifetime of about 20%. We validate that this change in lifetime is due to a superradiant rate enhancement by confirming the simultaneous presence of an antidip in the HBT data, which indicates the presence of interemitter coherences. Additionally, we investigate a region of intermediate detunings, where photon correlations show nonclassical behavior even at detunings of several single-emitter linewidths, while no changes were observed in decay rate. Therefore, our experiments reveal that correlations are still present at very large detunings, where no change in the decay rate is observed, or expected.

Acknowledgements. D.H., M.S.S., and L.R.W. acknowledge support from UK EPSRC (Grant No. EP/V026496/1). M.C. is supported by the Return Program of the State of North Rhine-Westphalia. E.M.G. acknowledges support from UK EPSRC (Grant No. EP/T01377X/1) and from the Leverhulme Trust (RPG-2022-335).

D.H. and L.H. performed the experiments. J.W., M.C., and E.M.G. developed the theoretical model. D.H, L.R.W, S.S., and A.F. contributed to the conception of the project. L.H., D.H., and N.M. designed the photonic devices. R.D. fabricated the photonic devices. I.F. and A.K.V. carried out the growth of the wafer. D.H. and J.W. wrote the letter, with contributions from all co-authors. L.R.W and M.S.S. supervised the project.

Data Availability. The data that supports the findings of this letter is openly available [54].

Supplementary References. References [55–57] are used exclusively in the supplementary information.

[1] R. H. Dicke, Coherence in spontaneous radiation processes, Phys. Rev. **93**, 99 (1954).

[2] A. Goban, C.-L. Hung, J. D. Hood, S.-P. Yu, J. A. Muniz, O. Painter, and H. J. Kimble, Superradiance for atoms trapped along a photonic crystal waveguide, Phys. Rev. Lett. **115**, 063601 (2015).

[3] V. V. Temnov and U. Woggon, Photon statistics in the cooperative spontaneous emission, Opt. Express **17**, 5774 (2009).

[4] A. Imamoğlu, D. D. Awschalom, G. Burkard, D. P. DiVincenzo, D. Loss, M. Sherwin, and A. Small, Quantum information processing using quantum dot spins and cavity QED, Phys. Rev. Lett. **83**, 4204 (1999).

[5] A. Aspuru-Guzik and P. Walther, Photonic quantum simulators, Nat. Phys. **8**, 285 (2012).

[6] W. S. Liu and P. Tombesi, Squeezing in a super-radiant state, Quantum Opt: J. Eur. Opt. Soc. Part B **3**, 93 (1991).

[7] D. Pagel, A. Alvermann, and H. Fehske, Nonclassical light from few emitters in a cavity, Phys. Rev. A **91**, 043814 (2015).

[8] J. A. Mlynek, A. A. Abdumalikov, C. Eichler, and A. Wallraff, Observation of Dicke superradiance for two artificial atoms in a cavity with high decay rate, Nat. Commun. **5**, 5186 (2014).

[9] A. González-Tudela and D. Porras, Mesoscopic entanglement induced by spontaneous emission in solid-state quantum optics, Phys. Rev. Lett. **110**, 080502 (2013).

[10] B. Julsgaard and K. Mølmer, Measurement-induced two-qubit entanglement in a bad cavity: Fundamental and practical considerations, Phys. Rev. A **85**, 032327 (2012).

[11] C. Gonzalez-Ballestero, A. Gonzalez-Tudela, F. J. Garcia-Vidal, and E. Moreno, Chiral route to spontaneous entanglement generation, Phys. Rev. B **92**, 155304 (2015).

[12] G. Buonaiuto, R. Jones, B. Olmos, and I. Lesanovsky, Dynamical creation and detection of entangled many-body states in a chiral atom chain, New J. Phys. **21**, 113021 (2019).

[13] A. Politi, J. C. F. Matthews, and J. L. O'Brien, Shor's quantum factoring algorithm on a photonic chip, Science **325**, 1221 (2009).

[14] D. E. Chang, J. S. Douglas, A. González-Tudela, C.-L. Hung, and H. J. Kimble, Colloquium: Quantum matter built from nanoscopic lattices of atoms and photons, Rev. Mod. Phys. **90**, 031002 (2018).

[15] J. Q. Quach, K. E. McGhee, L. Ganzer, D. M. Rouse, B. W. Lovett, E. M. Gauger, J. Keeling, G. Cerullo, D. G. Lidzey, and T. Virgili, Superabsorption in an organic microcavity: Toward a quantum battery, Sci. Adv. **8**, eabk3160 (2022).

[16] A. Rastogi, E. Saglamyurek, T. Hrushevskyi, and L. J. LeBlanc, Superradiance-mediated photon storage for broadband quantum memory, Phys. Rev. Lett. **129**, 120502 (2022).

[17] A. A. Kalachev, Quantum memory based on optical subradiance: Optimization of the signal-to-noise ratio, Bull. Russ. Acad. Sci.: Phys. **72**, 691 (2008).

[18] S. Davidson, F. A. Pollock, and E. Gauger, Eliminating radiative losses in long-range exciton transport, PRX Quantum **3**, 020354 (2022).

[19] A. Mattioni, F. Caycedo-Soler, S. F. Huelga, and M. B. Plenio, Design principles for long-range energy transfer at room temperature, Phys. Rev. X **11**, 041003 (2021).

[20] M. Gross and S. Haroche, Superradiance: An essay on the theory of collective spontaneous emission, Phys. Rep. **93**, 301 (1982).

[21] A. Tiranov, V. Angelopoulou, C. J. van Diepen, B. Schrinski, O. A. D. Sandberg, Y. Wang, L. Midolo, S. Scholz, A. D. Wieck, A. Ludwig, A. S. Sørensen, and P. Lodahl, Collective super- and subradiant dynamics between distant optical quantum emitters, Science **379**, 389 (2023).

[22] J. Wiercinski, M. Cygorek, and E. M. Gauger, Role of polaron dressing in superradiant emission dynamics, Phys. Rev. Res. **6**, 033231 (2024).

[23] M. Scheibner, T. Schmidt, L. Worschech, A. Forchel, G. Bacher, T. Passow, and D. Hommel, Superradiance of quantum dots, Nat. Phys. **3**, 106 (2007).

[24] D. Bhatti, J. von Zanthier, and G. S. Agarwal, Superbunching and nonclassicality as new hallmarks of superradiance, Sci. Rep. **5**, 17335 (2015).

[25] M. Cygorek, E. D. Scerri, T. S. Santana, Z. X. Koong, B. D. Gerardot, and E. M. Gauger, Signatures of cooperative emission in photon coincidence: Superradiance versus measurement-induced cooperativity, Phys. Rev. A **107**, 023718 (2023).

[26] J.-H. Kim, C. J. K. Richardson, R. P. Leavitt, and E. Waks, Two-photon interference from the far-field emission of chip-integrated cavity-coupled emitters, Nano Lett. **16**, 7061 (2016).

[27] S. Wolf, S. Richter, J. von Zanthier, and F. Schmidt-Kaler, Light of two atoms in free space: Bunching or antibunching? Phys. Rev. Lett. **124**, 063603 (2020).

[28] Z. X. Koong, M. Cygorek, E. Scerri, T. S. Santana, S. I. Park, J. D. Song, E. M. Gauger, and B. D. Gerardot, Coherence in cooperative photon emission from indistinguishable quantum emitters, Sci. Adv. **8**, eabm8171 (2022).

[29] J. Wiercinski, E. M. Gauger, and M. Cygorek, Phonon coupling versus pure dephasing in the photon statistics of cooperative emitters, Phys. Rev. Res. **5**, 013176 (2023).

[30] L. Zhai, M. C. Löbl, G. N. Nguyen, J. Ritzmann, A. Javadi, C. Spinnler, A. D. Wieck, A. Ludwig, and R. J. Warburton, Low-noise GaAs quantum dots for quantum photonics, Nat. Commun. **11**, 4745 (2020).

[31] L. Zhai, G. N. Nguyen, C. Spinnler, J. Ritzmann, M. C. Löbl, A. D. Wieck, A. Ludwig, A. Javadi, and R. J. Warburton, Quantum interference of identical photons from remote GaAs quantum dots, Nat. Nanotechnol. **17**, 829 (2022).

[32] P. Lodahl, S. Mahmoodian, and S. Stobbe, Interfacing single photons and single quantum dots with photonic nanostructures, Rev. Mod. Phys. **87**, 347 (2015).

[33] M. Arcari, I. Söllner, A. Javadi, S. Lindskov Hansen, S. Mahmoodian, J. Liu, H. Thyrrestrup, E. H. Lee, J. D. Song, S. Stobbe, and P. Lodahl, Near-unity coupling efficiency of a quantum emitter to a photonic crystal waveguide, Phys. Rev. Lett. **113**, 093603 (2014).

[34] J.-H. Kim, S. Aghaeimeibodi, C. J. K. Richardson, R. P. Leavitt, and E. Waks, Super-radiant emission from quantum dots in a nanophotonic waveguide, Nano Lett. **18**, 4734 (2018).

[35] J. Q. Grim, A. S. Bracker, M. Zalalutdinov, S. G. Carter, A. C. Kozen, M. Kim, C. S. Kim, J. T. Mlack, M. Yakes, B. Lee, and D. Gammon, Scalable in operando strain tuning

in nanophotonic waveguides enabling three-quantum-dot superradiance, Nat. Mater. **18**, 963 (2019).

[36] J. D. Hood, Atom-light interactions in a photonic crystal waveguide, Ph.D. thesis, California Institute of Technology, 2017.

[37] A. Albrecht, L. Henriet, A. Asenjo-Garcia, P. B. Dieterle, O. Painter, and D. E. Chang, Subradiant states of quantum bits coupled to a one-dimensional waveguide, New J. Phys. **21**, 025003 (2019).

[38] A. Asenjo-Garcia, M. Moreno-Cardoner, A. Albrecht, H. J. Kimble, and D. E. Chang, Exponential improvement in photon storage fidelities using subradiance and "selective radiance" in atomic arrays, Phys. Rev. X **7**, 031024 (2017).

[39] X.-L. Chu, V. Angelopoulou, P. Lodahl, and N. Rotenberg, Subradiant states for two imperfect quantum emitters coupled by a nanophotonic waveguide, Phys. Rev. A **106**, 053702 (2022).

[40] A. Sipahigil, R. E. Evans, D. D. Sukachev, M. J. Burek, J. Borregaard, M. K. Bhaskar, C. T. Nguyen, J. L. Pacheco, H. A. Atikian, C. Meuwly, R. M. Camacho, F. Jelezko, E. Bielejec, H. Park, M. Lončar, and M. D. Lukin, An integrated diamond nanophotonics platform for quantum-optical networks, Science **354**, 847 (2016).

[41] X.-L. Chu, C. Papon, N. Bart, A. D. Wieck, A. Ludwig, L. Midolo, N. Rotenberg, and P. Lodahl, Independent electrical control of two quantum dots coupled through a photonic-crystal waveguide, Phys. Rev. Lett. **131**, 033606 (2023).

[42] H. S. Nguyen, G. Sallen, C. Voisin, P. Roussignol, C. Diederichs, and G. Cassabois, Optically gated resonant emission of single quantum dots, Phys. Rev. Lett. **108**, 057401 (2012).

[43] H. S. Nguyen, G. Sallen, M. Abbarchi, R. Ferreira, C. Voisin, P. Roussignol, G. Cassabois, and C. Diederichs, Photoneutralization and slow capture of carriers in quantum dots probed by resonant excitation spectroscopy, Phys. Rev. B **87**, 115305 (2013).

[44] See Supplemental Material at http://link.aps.org/supplemental/10.1103/1xsb-bf5r for a more detailed derivation of the analytical expressions as well as information about the numerically exact calculations (2025).

[45] C. M. Lalau-Keraly, S. Bhargava, O. D. Miller, and E. Yablonovitch, Adjoint shape optimization applied to electromagnetic design, Opt. Express **21**, 21693 (2013).

[46] J. Wang, Y. Shi, T. Hughes, Z. Zhao, and S. Fan, Adjoint-based optimization of active nanophotonic devices, Opt. Express **26**, 3236 (2018).

[47] F. T. Pedersen, Y. Wang, C. T. Olesen, S. Scholz, A. D. Wieck, A. Ludwig, M. C. Löbl, R. J. Warburton, L. Midolo, R. Uppu, and P. Lodahl, Near transform-limited quantum dot linewidths in a broadband photonic crystal waveguide, ACS Photonics **7**, 2343 (2020).

[48] M. N. Makhonin, J. E. Dixon, R. J. Coles, B. Royall, I. J. Luxmoore, E. Clarke, M. Hugues, M. S. Skolnick, and A. M. Fox, Waveguide coupled resonance fluorescence from on-chip quantum emitter, Nano Lett. **14**, 6997 (2014).

[49] A. Auffèves, D. Gerace, S. Portolan, A. Drezet, and M. F. Santos, Few emitters in a cavity: from cooperative emission to individualization, New J. Phys. **13**, 093020 (2011).

[50] L. Sapienza, M. Davanço, A. Badolato, and K. Srinivasan, Nanoscale optical positioning of single quantum dots for bright and pure single-photon emission, Nat. Commun. **6**, 7833 (2015).

[51] P. Schnauber, J. Schall, S. Bounouar, T. Höhne, S.-I. Park, G.-H. Ryu, T. Heindel, S. Burger, J.-D. Song, S. Rodt, and S. Reitzenstein, Deterministic integration of quantum dots into on-chip multimode interference beamsplitters using in situ electron beam lithography, Nano Lett. **18**, 2336 (2018).

[52] T. Pregnolato, X.-L. Chu, T. Schröder, R. Schott, A. D. Wieck, A. Ludwig, P. Lodahl, and N. Rotenberg, Deterministic positioning of nanophotonic waveguides around single self-assembled quantum dots, APL Photonics **5**, 086101 (2020).

[53] Y. Hou, A review of site-controlled compound semiconductor quantum dots for single photon emitters, Mater. Quantum Technol. **5**, 032001 (2025).

[54] The dataset for this article is available at https://doi.org/10.15131/shef.data.27902034.

[55] H.-P. Breuer and F. Petruccione, *The Theory of Open Quantum Systems* (Oxford University Press, Oxford, 2007), 1st ed.

[56] Z. Ficek and S. Swain, *Quantum Interference and Coherence: Theory and Experiments*, Springer Series in Optical Sciences No. 100 (Springer, New York, Heidelberg, 2005).

[57] J. V. Wall and C. R. Jenkins, *Practical Statistics for Astronomers* (Cambridge University Press, Cambridge, 2012).